LA-UR -85-3166

OCT 09 1985

CONF-8509560--11

LA-UR--85-3166

DE86 000782

TITLE: *THREE-DIMENSIONAL SIMULATIONS OF FREE-ELECTRON LASER PHYSICS*

AUTHOR(S): *B. D. McVey, X-1*

SUBMITTED TO. *Seventh International Free-Electron Laser Conference*
September 8 -13, 1985
Tahoe City, CA

Los Alamos Los Alamos National Laboratory
Los Alamos, New Mexico 87545

FORM NO 836 R4
ST NO 2629 5/81

THREE-DIMENSIONAL SIMULATIONS OF FREE-ELECTRON LASER PHYSICS *

B. D. MCVEY
Los Alamos National Laboratory, University of California, Los Alamos, NM 87545

A computer code has been developed to simulate three-dimensional free-electron laser physics. A mathematical formulation of the FEL equations is presented, and the numerical solution of the problem is described. Sample results from the computer code are discussed.

1. Introduction

A computer code has been developed at Los Alamos that simulates three-dimensional free-electron laser physics. The calculation is based upon the Monte Carlo technique of following the orbits of individual electrons, and then evaluating the macroscopic current to determine the interaction with the optical field. For a linear undulator, we assume the usual coordinate system where x is the wiggle direction, y is the direction of the magnetic field, and z is the axis of the laser. The electron orbits are determined by numerically solving the relativistic Lorentz force equation [1]. Included in the electron beam dynamics are the following: 1) finite emittance (an arbitrary initial electron distribution in x, β_x, y, β_y), 2) energy spread (distribution in γ), 3) wiggler focussing of the electron beam in the y-direction (betatron motion) , 4) and wiggle plane (x-plane) focussing either due external quadrapoles or due to parabolic pole faces of the wiggler magnets [2]. Multiple optical wavefronts can be followed in the code. Along the z-axis, a finite width near the center of the optical pulse is modelled . Periodic boundary conditions [3] are imposed on those electrons that slip out of the end of the optical computational box and are re-injected at the front. The evolution of the optical field is determined by solving the paraxial wave equation [4] with an inhomogeneous driving term. The driving term is a result of the stimulated emission of the electron beam in the presence of the optical field. In the context of the periodic model of the optical field, the three-dimensional evolution of the sideband instability [5] can be studied. The computer code was developed to simulate the Los Alamos FEL oscillator experiments. At the end of the wiggler, the optical field is propagated through an optical resonator cavity to the wiggler entrance where the electron beam interaction is re-initiated. Multiple passes through the wiggler

* This work was performed under the auspices of the U. S. Department of Energy and partially supported by the U. S. Army Ballistic Missile Defense Organization.

results in a self-consistent 3-D FEL resonator solution.

The development of computer codes to simulate 3-D FEL physics is of particular importance in a number of FEL designs. Long amplifier designs (wiggler length many times longer than the optical Rayleigh range) require optical guiding [6]. The efficiency of electron capture and deceleration in the optical bucket is sensitive to the cross-sectional profile or diffraction of the optical beam along the length of the wiggler. Determining the feasibility of using an RF linac to drive an XUV-FEL ($\lambda < 2000$Å) is dependent upon proper modelling of the electron beam emittance [7]. The small signal gain curves as a function of wavelength are sensitive to the initial distribution of electrons in x, β_x, y, and β_y. Finally for FEL oscillator systems, 3 D FEL simulations are required to evaluate: 1) the sensitivity of performance with electron-optical beam misalignments, 2) optical beam quality, and 3) self-consistent resonator optical cavity solutions.

A number of researchers have developed or are in the process of developing computer codes that simulate 3-D FEL physics [8-13]. Two basic approaches are used to represent the optical field. The optical field can be represented as an expansion of normal (Gaussian) modes [12-13], or the field is represented by a set of discrete values on a planar grid [8-11]. In this work, we use the latter representation. Advantages of this approach are; 1) the generality in representing non-Gaussian optical field profiles which includes the effects of aperturing the field, 2) compatibility with many optical codes for use in the design of optical resonators [11], and 3) compatibility with arbitrary initial electron distributions. The disadvantage of the discrete representation is the attendent requirement of more computer time. As described in the first paragragh, the 3-D FEL computer code descrided here was structured to include as much physics as feasible. As an example, the Los Alamos oscillator experiments have an elliptical electron beam with an energy spread, and a broad (5%) optical spectrum is observed. The 3-D FEL code described here models these effects except for the overall shape (along z) of the optical pulse. Presently, a full pulse calculation would require an excessive amount of computer time so a comprimize has been made and only the center of the optical pulse is modelled.

The remainder of this paper is orgainized as follows. In the next section, the mathematical formulation of the particle and field equations is presented. In section 3, the numerical solution of the problem is described. In Section 4, sample results from the computer code are discussed.

Finally, some conclusions and discussion are presented in the final section.

2. Mathematical Formulation of the FEL Equations

The individual electron equations of motion follow from averaging the relativistic Lorentz force equation over the spatial period of the undulator [14]. An optical field of the following form is assumed.

$$E_x(\vec{r},t) = E_o(\vec{r})\cos\left[k_o z - \omega t + \theta_o(\vec{r})\right] \tag{1}$$

where E_o is the magnitude and θ_o the phase of the optical field both of which are slowly varying functions of x, y, and z. For the assumed form of the optical field, the energy equation for the electrons has the form,

$$\frac{d\gamma}{d(ct)} = \frac{e}{mc^2}\frac{a_w(\vec{r})}{2\gamma}F_\mu E_o(\vec{r})\cos\left[\psi + \theta_o(\vec{r})\right] \tag{2}$$

$$F_\mu = J_0(\mu) - J_1(\mu) \quad , \quad \mu = \frac{k_o a_w}{16\gamma^2 k_w} \tag{2a}$$

In Eq. 2, $a_w(\vec{r}) = (eB_w(\vec{r}))/(mc^2 k_w)$ is the normalized vector potential of the wiggler. The 3-D wiggler field is approximated as [2],

$$\chi_m = -\frac{B(z)}{k_{wy}}\cosh(k_{wx}x)\sinh(k_{wy}y)\sin\left[\int k_w(z)dz\right] \tag{3a}$$

$$\vec{B}_w = -\nabla\chi_m \quad , \quad {k_w}^2 = {k_{wx}}^2 + {k_{wy}}^2 \tag{3b}$$

For linear magnets with no focussing in the x direction, $k_{wx} = 0, k_{wy} = k_w$. For parabolic pole face magnets with equal focussing in the x and y directions, $k_{wx} = k_{wy} = k_w/\sqrt{2}$. The electrons slip behind a fixed point on the optical pulse, a distane $\delta_s = \int \beta_z dt - ct$ after a time interval, t. The differential equation describing the slippage has the form,

$$\frac{d\delta_s}{d(ct)} = -\frac{1}{2\gamma^2}\left[1 + \frac{a_w(\vec{r})^2}{2} + (\gamma\beta_x)^2 + (\gamma\beta_y)^2\right] \tag{4}$$

In Eq. 2, ψ is the relative phase of the electron wiggle motion to that of the optical field oscillations,

$$\psi(z) = \int k_w(z)dz + k_o\delta_s \tag{5}$$

The transverse motion of the electrons is determined by the following equations consistent with the assumed form for the wiggler field.

$$\frac{d(\gamma\beta_x)}{d(ct)} = -\frac{{a_w}^2{k_{wx}}^2}{2\gamma}x - \frac{e}{mc^2}(\beta_y B_z^s - \beta_z B_y^s) \tag{6}$$

$$\frac{d(\gamma\beta_y)}{d(ct)} = -\frac{{a_w}^2{k_{wy}}^2}{2\gamma}y - \frac{e}{mc^2}(\beta_z B_x^e - \beta_x B_z^e) \tag{7}$$

$$\frac{dx}{d(ct)} = \beta_x \quad , \quad \frac{dy}{d(ct)} = \beta_y \tag{8}$$

The quantities B_x^e, B_y^e, and B_z^e represent external focussing coils such as a quadrapole set [2,15]. Equations 2, and 4-8 describe the electron trajectories in the presence of an optical and wiggler magnetic field.

The optical field is driven by the currents deduced from the set of electron equations. From Maxwell's equations we derive [16],

$$\mathbf{E} = E_o(\vec{r})\exp[i\theta_o(\vec{r})] \tag{9a}$$

$$2ik_o\frac{\partial \mathbf{E}}{\partial z} + \frac{\partial^2 \mathbf{E}}{\partial x^2} + \frac{\partial^2 \mathbf{E}}{\partial y^2} = S(\vec{r}) \tag{9b}$$

$$S(\vec{r}) = \left\langle -\frac{4\pi i k_o}{c} J \frac{a_w}{\gamma} F_\mu e^{-i(\psi+\theta_o)} \right\rangle e^{i\theta_o} \tag{9c}$$

where J is the electron current density and the brackets represent an average of all the electrons at the position $\vec{r}$.

The above set of equations uniquely define a solution for a given FEL configuration if; 1) initial conditions on $(\gamma, \psi, \beta_x, x, \beta_y y)$ are specified for each electron at the entrance to the wiggler, and 2) boundary conditions are imposed on $\mathbf{E}$ at the entrance and along the sides of the wiggler. The magnitude of the electron beam emittance and a model five-dimensional distribution function defines the initial conditions on each electron. The model distribution assumed for the results presented in this paper is product of uncorrelated Gaussians characterized by average $(\gamma^0, \beta_x^0, x^0, \beta_y^0, y^0)$ and r.m.s. $(\gamma^1, \beta_x^1, x^1, \beta_y^1, y^1)$ parameters. The average values allow for electron beam misalignment from the optical axis. For the Gaussian distribution, the electron beam emittance is defined in terms of the r.m.s. values,

$$\epsilon_x = \pi\beta_x^1 x^1 \quad , \quad \epsilon_y = \pi\beta_y^1 y^1 \tag{10a}$$

In the y-direction, we assume the beam is matched for a constant envelope along the wiggler axis.

$$y^1 = \left(\frac{\sqrt{2\gamma}\epsilon_y}{\pi a_w k_{wy}}\right)^{\frac{1}{2}} \quad , \quad \beta_y^1 = \frac{\epsilon_y}{\pi y^1} \tag{10b}$$

For the x direction, the initial distribution is sent through an ideal thin lens which focusses the beam at the center of the wiggler. Figure 1 illustrates the electron beam size through the wiggler for the parameters listed in Table 1.

At the wiggler entrance and for the initial pass of light, the transverse profile of the electric field is set equal to that of a Gaussian beam characterized by a wavelength, a focal position, and a Rayleigh range. Subsequent passes through the wiggler use the electric field profiles generated on the previous pass after propagation through the cavity. The boundary conditions imposed on the sides of the wiggler require the electric field to be zero. Typically, the square window used for the optical field is three times the size of the electron beam.

3. Numerical Solution of the FEL Equations

The numerical solution to the equations presented in Section 2 divides itself into three parts; 1) an algorithm for the set of ordinary differential equations describing the electron motion, 2) an algorithm for the parabolic partial differential equation governing the optical field, and 3) the connection between 1) and 2). The electrons are advanced along their trajectories by various order (2,3,4) Runge-Kutta algorithms [17]. The Runge-Kutta algorithms were chosen to minimize the requirements on computer memory, and are compatible with minimal reading and writing of the electron parameters to disc when performing simulations with a large number of electrons. The electron initial conditions are obtained by using statified sampling [18] of the assumed model distribution. A finite-difference alternating direction implicit (ADI) method [17] is used to construct a solution to the paraxial wave equation. An increased accuracy five-point expression is used to approximate the x and y partials in Eq. 9b.

The connection between the optical field and the electron motion is through the source term ($S(\vec{r})$) in Eq. 9. For a given time step, the optical field is advanced first using a fourth order Adams-Bashforth predictor formula [17] to estimate the source function in the time interval. The electrons are then advanced using bilinear interpolation to evaluate the electric field at the electron position from the discrete grid of electric field values. The source function at the new time is then evaluated, and the above process is repeated. An option exists in the computer code for a corrector formula to be used in recalculating the electric field after a time step. This provides a check on

the accuracy of the above numerical procedure. Usually, a small time step is selected such that the predictor formula provides sufficient accuracy. Outside the wiggler, the optical field is propagated through the resonant cavity using standard fast Fourier transform algorithms [19].

4. Sample Results

Two examples are presented that illustrate some of the results that are obtainable with the Los Alamos 3-D FEL computer code. The assumed FEL parameters are listed in Table 1. The parameters are typical of those expected in the ERX experiment [20] at Los Alamos. An untapered wiggler magnetic field is assumed. The first example is to generate the self-consistent FEL resonator solution for a single wavefront for the two resonant cavities listed in the Table. The first cavity is the experimental cavity to be used in the ERX experiments. The second cavity is a near concentric cavity that is more typical of future higher power FEL experiments. The second example is three-dimensional modelling of the sideband instability.

We consider a theoretical FEL oscillator configuration which models the Los Alamos FEL oscillator experiment. The RF linac produces, typically, two thousand electron micro-pulses which pass through the wiggler and generate light. We assume perfect synchronism between the electron beam and the arrival of the light which was generated on the previous pass. In such a configuration, the optical field builds up from spontaneous emission to a saturated power level consistent with the electron beam parameters and the resonant cavity. In the computer code, the initial optical wavefront is assumed to be at a power level in the small signal gain regime, however well above the noise level. The amplitude and phase curvature of the initial optical wave front are assumed to match the empty resonant cavity mode. Figures 2a and b illustrate the optical field build-up for the g=.87 cavity in Table 1. The power reaches saturation at a level of 120 Mw. peak for an output coupling fraction of twenty percent. The oscillations observed on the optical gain curve indicates that the initial optical wavefront (empty cavity mode) does not match the self-consistent FEL resonator field solution. In addition to gain, the electron beam acts like an optical lens. Shown in Figures 3a and 3b is the optical phase front after pass number one, and the cross-sectional amplitude of the optical beam for the last pass (number 60). It is observed that the radius of curvature of the wave form is narrower 70 cm. at the exit of the wiggler compared to an input

radius of curvature of 130 cm. At saturation, the cross-sectional amplitude of the optical beam is very close to that of a Gaussian beam as illustrated in Fig 3b. The period of oscillation of the optical gain curve can be explained in terms of a unilateral simple lens [21]. In the Los Alamos FEL experiments, observations of oscillations in the optical power decay after turn-off of the electron beam have been attributed to refractive and diffractive effects of the FEL interaction [21].

For the near concentric cavity (g=.993), the optical field builds up to a power level slightly higher than that of the g=.87 cavity. The saturated cross-sectional profile of the optical field is illustrated in Fig. 4. For the concentric cavity, there is slightly more distortion away from the reference Gaussian beam (i.e. there is larger content of higher order cavity modes [8]). The sensitivity of FEL operation to mirror tilt is illustrated in Table 2. The factor ϵ is defined as the angle of the optical axis divided by the half angle of the optical beam ($\epsilon = R\theta_m \pi w_o/(2R - l)\lambda$). For rather large values of ϵ there is reasonably small decrease in the saturated optical power. The FEL operation seems to be more insensitive to mirror tilt than the simple criterion ($\epsilon << 1.$) would suggest.

As a last example, the 3-D FEL code was run with 16 optical wavefronts to investigate the side-band instability in three dimensions. The parameters of Table 1 with the g=.87 cavity were assumed. The simulation was started at a relatively high on axis optical intensity ($I_o = 10^8 w/cm^2$) with a ten percent white noise. For these conditions, the sideband spectrum is well developed in a relatively small number of passes. Figures 5a-c illustrate the amplitude, phase, and spectrum of a section of optical wavefront (.064 cm. wide) over a x cross-sectional cut of the optical beam after 200 passes through the FEL. Strong amplitude and phase modulation is observed, and the spectrum has significant content in longer wavelength (lower) sidebands. The one striking feature is that the wavefront amplitude and the spectrum appear Gaussian in x. Furthermore, the phase fronts are parabolic which suggests good optical beam quality in the presence of the sideband instability. This result is consistent with the experimental observations in the Los Alamos FEL oscillator experiments [22]. There are two probable reasons for the good optical beam quality observed in Fig 5. First, the output coupling is only two percent for these simulation results. With only two percent of additional light generated per pass, there is a minor change in the established fundamental Gaussian mode of the cavity. Second, the electron beam is relatively small compared

to the width of the optical beam. The gain of light is largest on axis where most of the electrons see the same electric field and have the same synchrotron period. As it propagates through the cavity, the light diffracts from the axis to fill out the Gaussian mode. Shown in the last figure is the electron energy extraction efficiency as a function of pass number. For a single optical wavefront, the theoretical maximum extraction efficiency is 1.25 percent. This value of extraction is close to the initial peak observed in Fig. 6. At this point, a majority of the electrons undergo one half of a synchrotron oscillation. As the optical field in the cavity continues to increase the extraction decreases as the electrons begin to fill the phase space of the optical field bucket. Finally as the sideband develops, the optical power begins to increase. The development of the sideband is seen to enhance the electron extraction efficiency for the untapered wiggler. A result which is consistent with experimental observations [23].

5. Conclusions and Discussion

We have presented a description and sample results from a computer code that simulates three-dimensional FEL physics. The orientation of the code development was toward modelling the relavent physics in the Los Alamos FEL oscillator experiments. This includes an electron beam with a finite emittance and elliptical cross-section, and a relatively broad optical field spectrum. The sample results presented here are preliminary (especially the sideband calculation), however the examples illustrate a number of questions that may be addressed with a 3-D simulation code. The utility of 3-D simulations of a FEL configuration is dependent upon the computer time needed for the calculation. A major and continuing effort has been made to select numerical algorithms and to properly structure the formulation in order to optimize performance on the CRAY computer systems.

The author has benefited from many discussions with members of the Los Alamos FEL program, C. J. Elliott, D. Feldman, J. C. Goldstein, K. Lee, B. E. Newnam, and R. W. Warren.

References

[1] H. Goldstein, Classical Mechanics, (Addison-Wesley, Reading, MA, 1950).

[2] E. T. Scharlemann, Lawrence Livermore National Laboratory Report No. UCRL-92429, (1985).

[3] W. B. Colson, Proc. Orcas Island FEL Workshop, eds. C. A. Brau, S. F. Jacobs, and M. O. Scully, SPIE vol. 453 (1984) 290.

[4] A. Yariv, Introduction to Optical Electronics, (Holt, Rinehart, and Winston, New York, NY, 1971).

[5] N. M. Kroll and M. N. Rosenbluth, Physics of Quantum Electronics, vol. 7 eds. S. F. Jacobs, M. Sargent, and M. O. Scully, (Addison-Wesley, Reading, MA, 1978) 157.

[6] E. T. Scharlemann, A. M. Sessler, and J. S. Wurtele, Lawrence Livermore National Laboratory Report No. UCRL 91476, (1984).

[7] J. C. Goldstein, B. E. Newnam, R. K. Cooper, J. S. Fraser, and J. C. Comley, Laser Techniques in the Extreme Ultraviolet, eds. S. E. Harris and T. B. Lucatorto, AIP Conf. Proc. No. 119 (Amer. Inst. of Physics, New York, 1984) 293.

[8] D. C. Quimby, and J. M. Slater, IEEE J. Quantum Electron. QE-19 (1983) 800.

[9] W. M. Fawley, D. Prosnitz, and E. T. Scharlemann, Phys. Rev. A30 (1984) 2472.

[10] A. Bhowmik and R. A. Cover, Proc. Orcas Island FEL Workshop, eds. C. A. Brau, S. F. Jacobs, and M. O. Scully, SPIE vol. 453 (1984) 218.

[11] D. R. Rossbach, Three-Dimensional, Spectrally-Resolved Engineering Model of a Free-Electron Laser, PhD Thesis, University of New Mexico, (1984).

[12] C. M. Tang and P. Sprangle, Proc. of the 1984 Free Electron Laser Conference, Castelgandolfo, Italy (1984) 61.

[13] M. N. Rosenbluth, H. V. Wong, and B. N. Moore, Austin Research Associates Report No. I-ARA-84-U-121, (1984).

[14] W. B. Colson, Physics of Quantum Electronics, vol. 5, eds. S. F. Jacobs, M. Sargent, and M. O. Scully, (Addison-Wesley, Reading, MA. 1978) 157.

[15] T. F. Wang and R. K. Cooper, Los Alamos Natioal Laboratory Report No. AT-6:ATN-84-15, (1984).

[16] W. B. Colson and S. K. Ride, Physics of Quantum Electronics, vol. 7, eds. S. F. Jacobs, H. S. Pillof, M. Sargent, M. O. Scully, and R. Spitzer, (Addison-Wesley, Reading, MA. 1978) 377.

[17] M. K. Jain, Numerical Solution of Diferential Equations, (John Wiley and Sons, New York, NY, 1979).

[18] J. M. Hammersley and D. C. Handscomb, Monte Carlo Methods, (Barnes and Noble, New York, NY, 1964).

[19] E. A. Sziklas and A. E. Siegman, Applied Optics, 14, (1975) 1874.

[20] R. W. Warren, private communication.

[21] R. W. Warren, these proceedings.

[22] B. E. Newnam, R. W. Warren, R. L. Sheffield, J. C. Goldstein, and C. A. Brau, Nuclear Instruments and Methods in Physics Research, A237 (1985) 187.

[23] R. W. Warren, J. C. Goldstein, and B. E. Newnam, these proceedings.

Table 1

FEL parameters used in the simulations.

Parameter:	Value:
electron beam,	
energy	42.6869
energy spread	1%
current	100. A.
emittance	$3. \times 10^{-4}$ cm-rad
wiggler,	
magnetic field	3. kG.
wavelength	2.73 cm.
length	100. cm.
optical,	
wavelength	$10\mu m$.
cavity 1:	g=.87
mirror positions	−369.2, 322.6 cm.
mirror curvature	−380., 335. cm.
cavity 2:	g=.993
mirror positions	-1200., 1200. cm.
mirror curvature	−1204., 1204. cm.

Table 2

FEL peak power as a function of mirror tilt.

θ_m	ϵ	Power
0. μrad	0.	140. Mw.
5.	.35	131.
10.	.70	111.
15.	1.05	80.
20.	1.4	44.

Figure Captions

Figure 1. Electron beam transport through the wiggler. The solid line is the x-width and the dotted line the y-width of the beam.

Figure 2. Build-up of optical power in the resonator. a) peak power in the cavity, b) percent gain per pass through the cavity.

Figure 3. a) Electric field phase profile after pass 1, b) the electric field amplitude profile at saturation for the g=.87 cavity.

Figure 4. The electric field amplitude profile at saturation for the near concentric cavity.

Figure 5. The optical profiles for multiple wavefronts. a) the optical pulse amplitude, b) the optical phase, and c) the optical spectrum.

Figure 6. The electron extraction efficiency as a function of pass number for the sideband simulation of Figure 5.

Figure 1

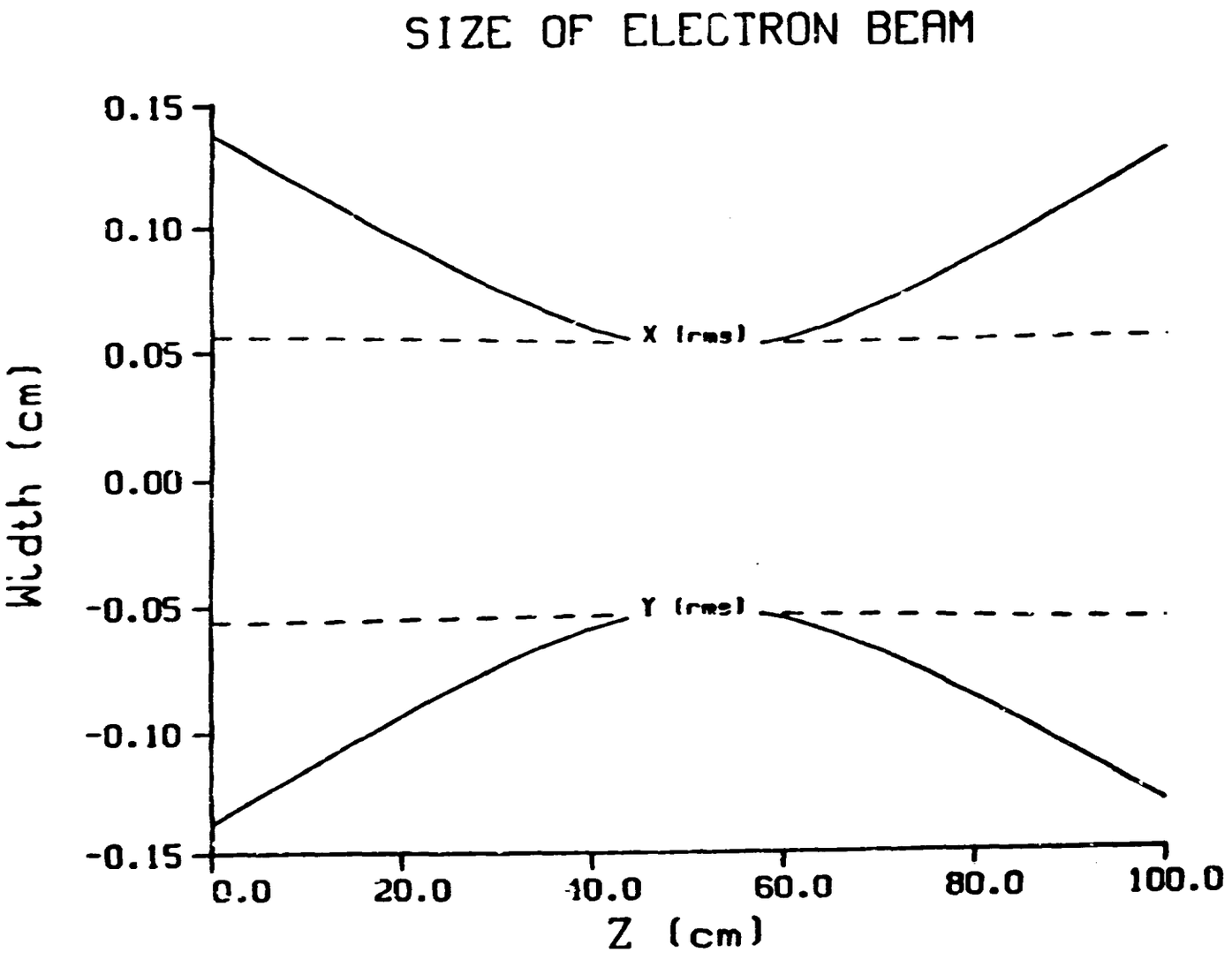
SIZE OF ELECTRON BEAM
0.15
0.10
0.05
0.00
-0.05
-0.10
-0.15
Width (cm)
X (rms)
Y (rms)
0.0
20.0
40.0
60.0
80.0
100.0
Z (cm)

Figure 2a

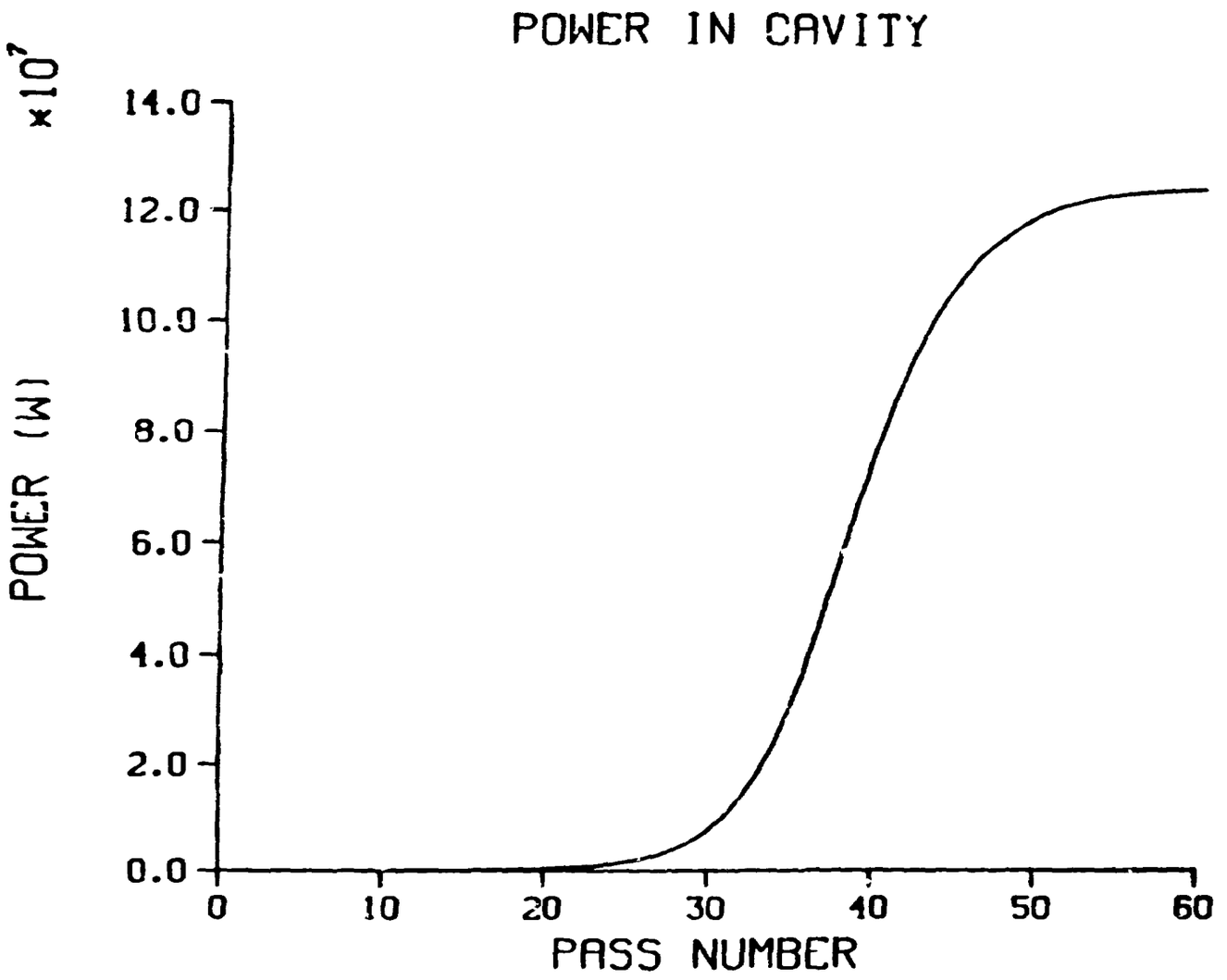
POWER IN CAVITY
POWER (W)
×10⁷
14.0
12.0
10.0
8.0
6.0
4.0
2.0
0.0
0
10
20
30
40
50
60
PASS NUMBER

Figure 2b

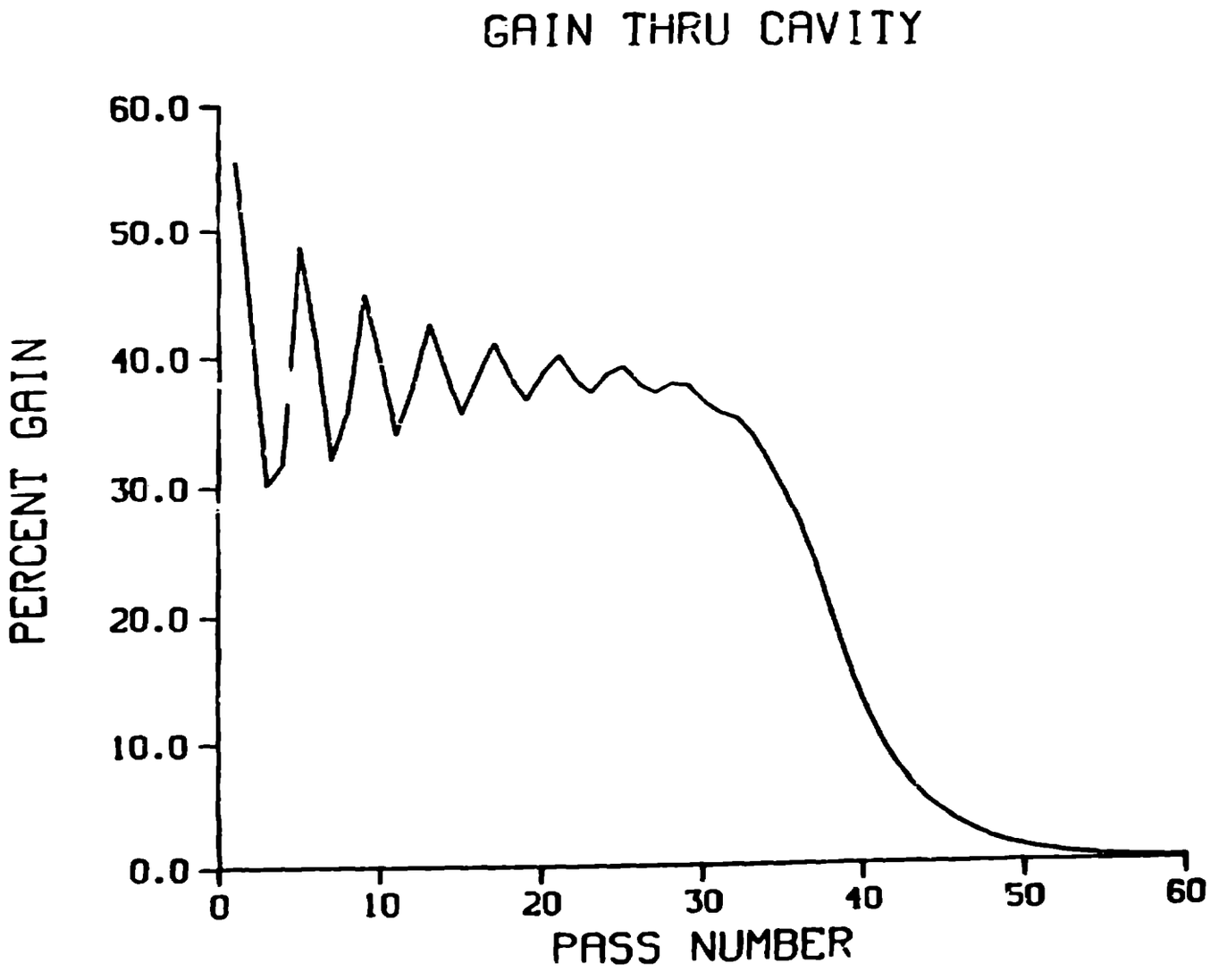
GAIN THRU CAVITY
PERCENT GAIN
60.0
50.0
40.0
30.0
20.0
10.0
0.0
0
10
20
30
40
50
60
PASS NUMBER

Figure 3a

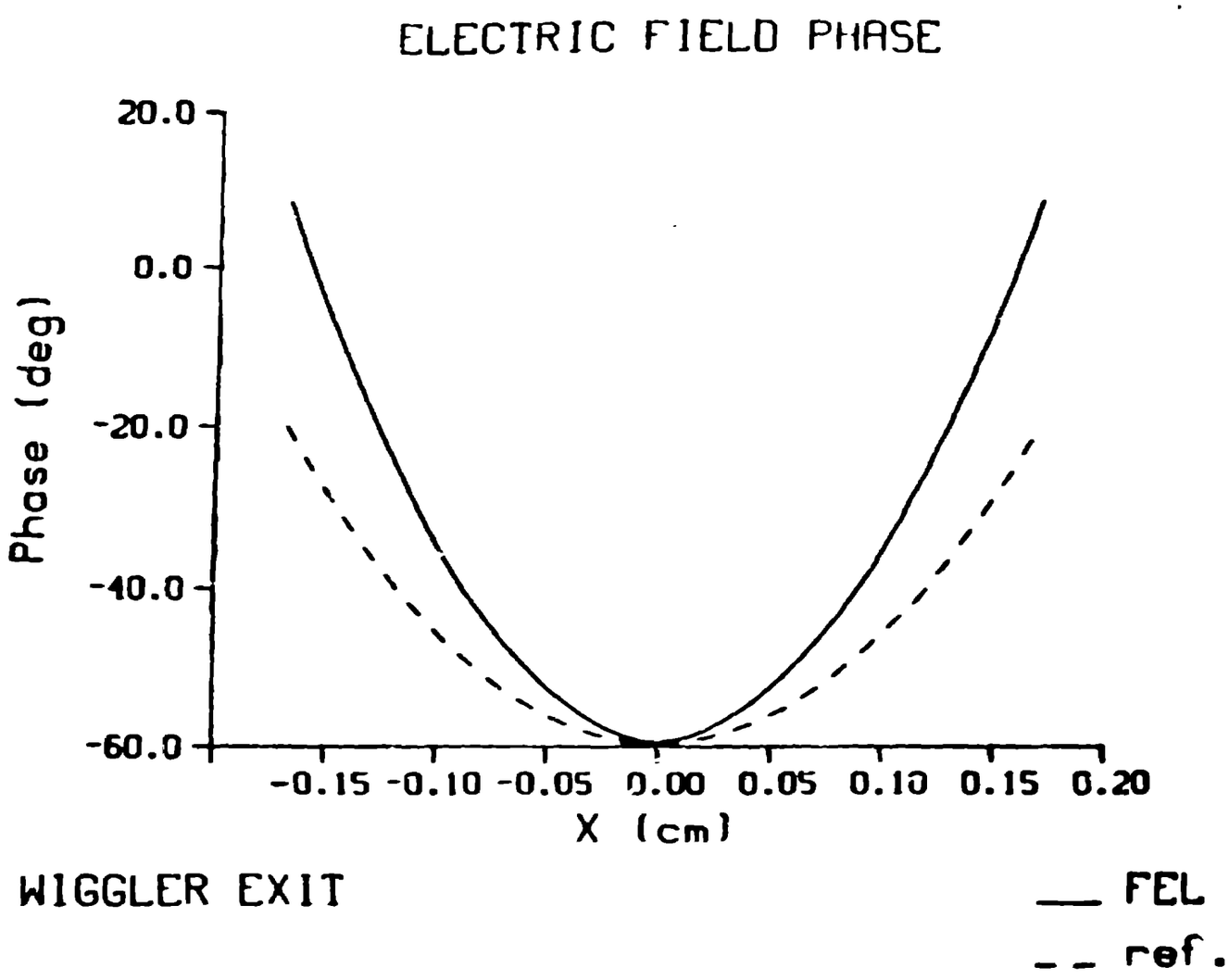
ELECTRIC FIELD PHASE
20.0
0.0
-20.0
-40.0
-60.0
Phase (deg)
-0.15 -0.10 -0.05 0.00 0.05 0.10 0.15 0.20
X (cm)
WIGGLER EXIT
FEL
ref.

Figure 3b

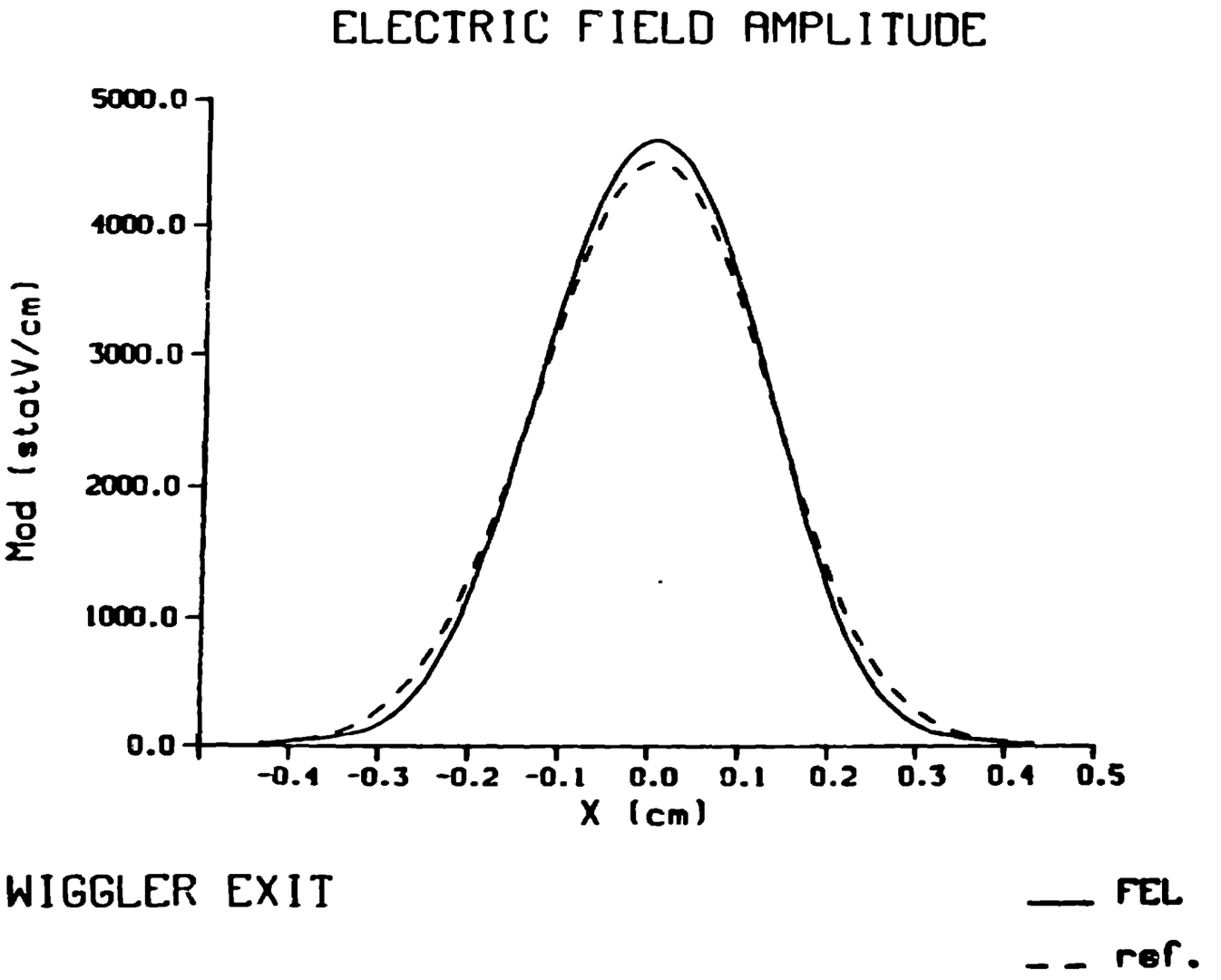
ELECTRIC FIELD AMPLITUDE
5000.0
4000.0
3000.0
2000.0
1000.0
0.0
Mod (statV/cm)
-0.4 -0.3 -0.2 -0.1 0.0 0.1 0.2 0.3 0.4 0.5
X (cm)
WIGGLER EXIT
FEL
ref.

Figure 4

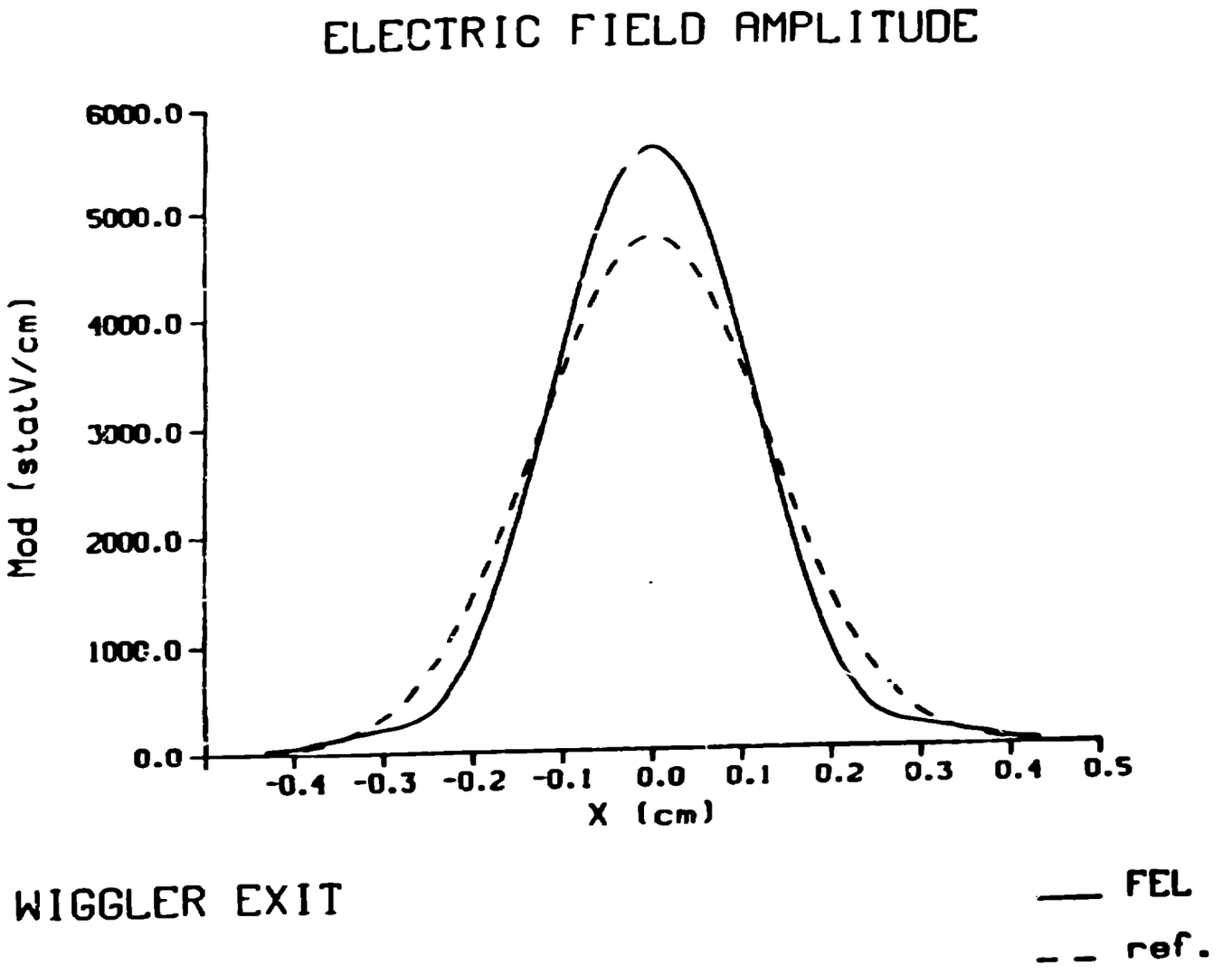
ELECTRIC FIELD AMPLITUDE
6000.0
5000.0
4000.0
3000.0
2000.0
1000.0
0.0
Mod (statV/cm)
-0.4 -0.3 -0.2 -0.1 0.0 0.1 0.2 0.3 0.4 0.5
X (cm)
WIGGLER EXIT
FEL
ref.

Figure 5a

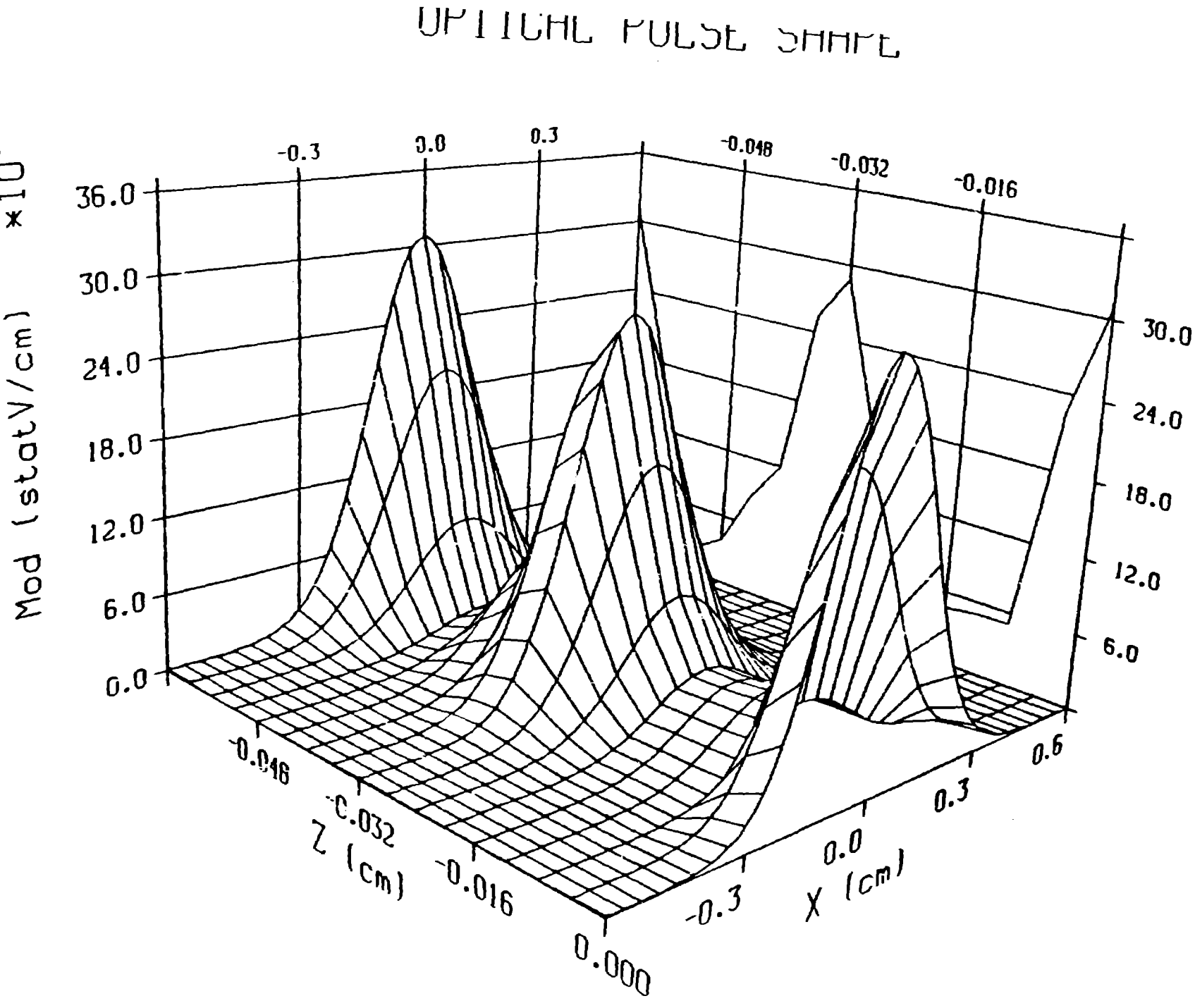
OPTICAL PULSE SHAPE
Mod (statV/cm) *10^3
36.0
30.0
24.0
18.0
12.0
6.0
0.0
-0.3
0.0
0.3
-0.048
-0.032
-0.016
30.0
24.0
18.0
12.0
6.0
-0.048
-0.032
-0.016
0.000
Z (cm)
-0.3
0.0
0.3
0.6
X (cm)

Figure 5b

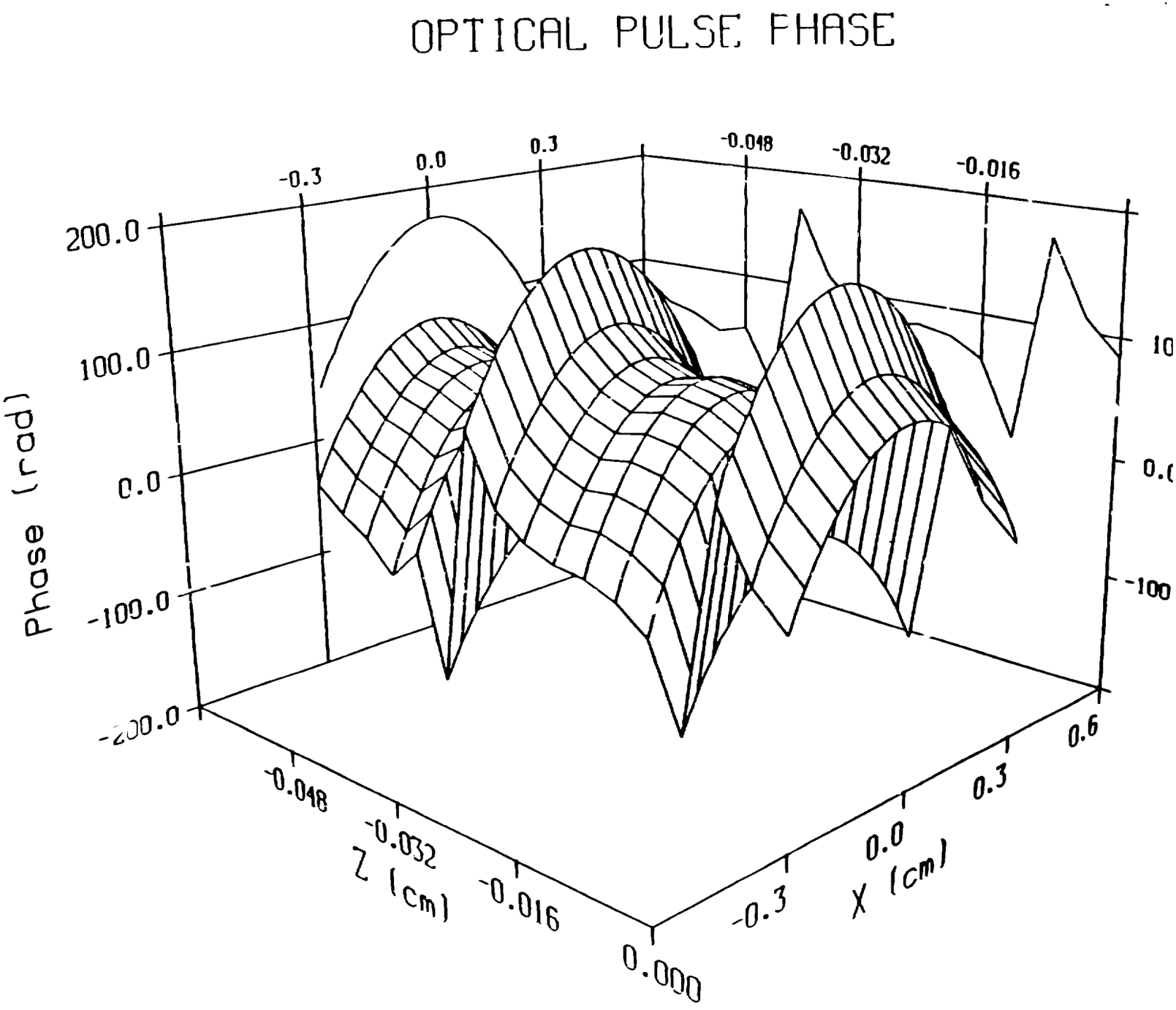
OPTICAL PULSE PHASE
-0.3
0.0
0.3
-0.048
-0.032
-0.016
200.0
100.0
0.0
-100.0
-200.0
Phase (rad)
10
0.(
-100
-0.048
-0.032
-0.016
0.000
Z (cm)
-0.3
0.0
0.3
0.6
X (cm)

Figure 5c

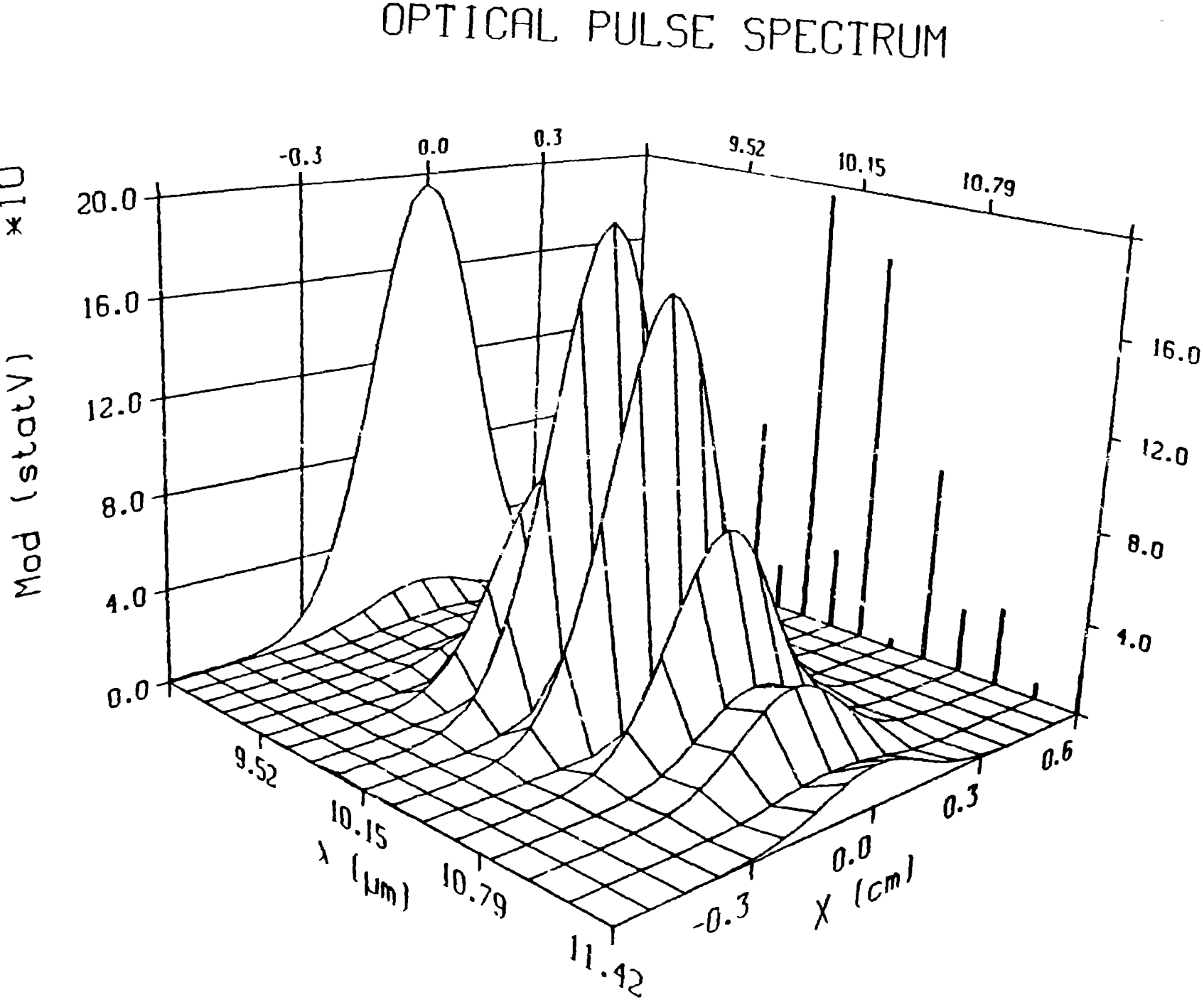
OPTICAL PULSE SPECTRUM
Mod (statV) *10^4
20.0
16.0
12.0
8.0
4.0
0.0
-0.3
0.0
0.3
9.52
10.15
10.79
16.0
12.0
8.0
1.0
9.52
10.15
λ (μm)
10.79
11.42
-0.3
0.0
X (cm)
0.3
0.6

Figure 6

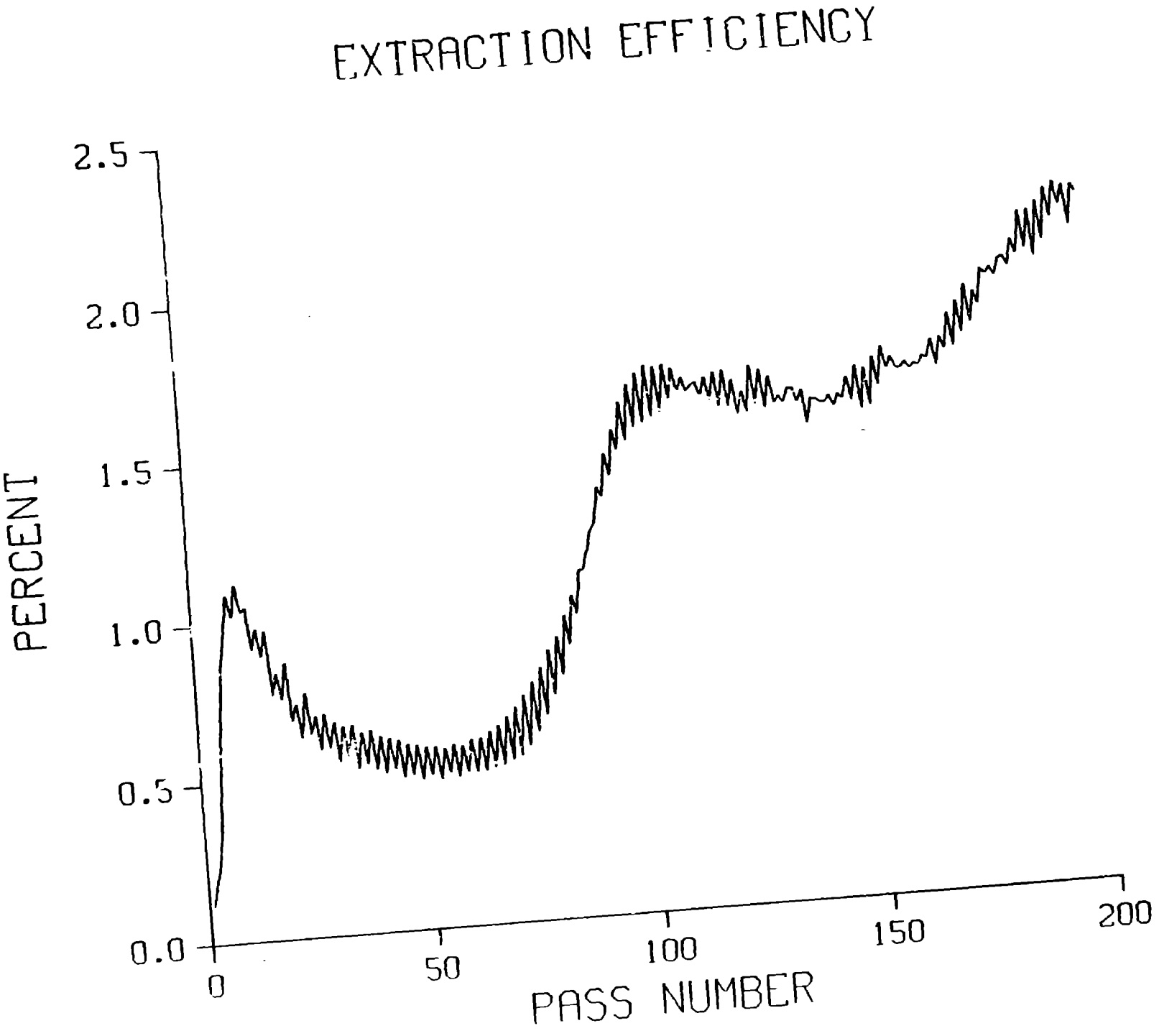
EXTRACTION EFFICIENCY
PERCENT
2.5
2.0
1.5
1.0
0.5
0.0
0
50
100
150
200
PASS NUMBER